

Spheroidal nanoparticles as thermal near-field sensors

Svend-Age Biehs*, Oliver Huth, Felix Rütting, and Martin Holthaus
Institut für Physik, Carl von Ossietzky Universität, D-26111 Oldenburg, Germany
(Dated: April 20, 2010)

We suggest to exploit the shape-dependence of the near-field heat transfer for nanoscale thermal imaging. By utilizing strongly prolate or oblate nanoparticles as sensors one can assess individual components of the correlation tensors characterizing the thermal near field close to a nanostructured surface, and thus obtain directional information beyond the local density of states. Our theoretical considerations are backed by idealized numerical model calculations.

PACS numbers: 44.40.+a, 78.67.-n, 05.40.-a, 41.20.Jb

Keywords: Near-field heat transfer, fluctuational electrodynamics, nanoscale thermal near-field imaging

I. INTRODUCTION

While profound theoretical understanding of thermally generated electromagnetic fields close to material surfaces has already been obtained some time ago [1–4], accurate experimental studies of such fluctuating thermal near fields at distances on the order of or even significantly shorter than the thermal wave length from a sample’s surface have only recently become possible. Hu *et al.* have measured the radiative heat flux between two glass plates spaced by a micron-sized gap [5], and reported near-field heat transfer exceeding the far-field limit set by Planck’s law of blackbody radiation. Chen and co-workers have studied the near-field heat flux between a sphere and a flat substrate [6, 7], focusing on the role of surface phonon polaritons, and observed heat transfer coefficients even three orders of magnitude larger than the blackbody radiation limit. Rousseau *et al.* have made precise measurements of the radiative heat transfer between spheres with diameters of 22 and 40 μm at distances from 30 nm to 2.5 μm from a plate [8], and obtained impressive agreement with predictions based on fluctuational electrodynamics [1, 2]. This finding is conceptually important since it indicates that fluctuational electrodynamics, which is a macroscopic theory, can be relied on at least up to the smallest distances accessible in this experiment, without having to account for effects caused by a nonlocal optical response [9, 10]. Moreover, a device termed Near-Field Scanning Thermal Microscope (NSThM) has been designed by Kittel *et al.* [11–13] This instrument allows one to record the near-field heat flux at probe-sample distances even down to a few nanometers, but still further efforts are required to achieve accurate calibration. A complementary set-up dubbed Thermal Radiation Scanning Tunneling Microscope (TRSTM) has enabled De Wilde *et al.* to take images of thermally excited surface plasmons, and to demonstrate spatial coherence effects in near-field ther-

mal emission [14]. This notable growth of experimental research on thermal near-field phenomena is triggered, on the one hand, by a wide variety of possible technological applications, ranging from the design of nanoscale heaters for use in heat-assisted magnetic recording or heat-assisted lithography [8] to near-field thermophotovoltaics [15–19]. On the other hand, there is a need for further insight into basic small-scale phenomena. For example, at very short distances nonlocal effects ultimately must come into play [9, 10], and the use of macroscopic fluctuational electrodynamics as a theoretical framework might no longer be sufficient. Thus, thermally induced near-field effects constitute an emerging subject which requires further experimental and theoretical investigations; of particular importance is the identification of experimentally observable quantities against which theoretical models can be tested.

It has already been demonstrated experimentally that the NSThM opens up the possibility of thermal imaging of surface structures with nanoscale resolution [20], since the surface topography leaves its imprint in the local density of states (LDOS). In this paper we take a further step in this direction: We argue that one can obtain information even beyond the mere topography if the NSThM sensor is appropriately shaped. This is due to the fact that in principle not only the LDOS, but even the individual diagonal components of the fluctuating fields’ correlation tensors are measurable; these components are singled out when employing strongly prolate or oblate spheroidal particles as sensors. Therefore, when scanning a surface at nanometer distances with such a sensor, the NSThM-signal does not give a one-to-one image of the surface profile, but rather provides information on how that profile affects the directional properties of the fluctuating thermal near field. We first sketch the theoretical idea underlying this proposal in Sec. II, and then present in Sec. III some numerical model calculations which illustrate its principal feasibility. These calculations necessarily are strongly idealized, and do not refer to an already existing experimental set-up; nonetheless, they indicate a possible direction for future developments.

*Present address: Laboratoire Charles Fabry, Institut d’Optique, CNRS, Université Paris-Sud, Campus Polytechnique, RD128, 91127 Palaiseau cedex, France

II. THE BASIC PRINCIPLE

Consider a substrate with temperature T_S . The electric field $\mathbf{E}(\mathbf{r}, t)$ close to its surface, generated by thermal fluctuations inside the sample, then is characterized in terms of its correlation tensor $W_{jk}^E(\mathbf{r}, \mathbf{r}', \omega)$, which is determined by an ensemble average

$$\langle E_j(\mathbf{r}, \omega) E_k^*(\mathbf{r}', \omega') \rangle = W_{jk}^E(\mathbf{r}, \mathbf{r}', \omega) \delta(\omega - \omega'), \quad (1)$$

where $E_j(\mathbf{r}, \omega)$ are the field's Fourier components. The magnetic correlation tensor $W_{jk}^H(\mathbf{r}, \mathbf{r}', \omega)$ is defined in an analogous manner. According to fluctuational electrodynamics [1, 2], these correlation tensors are proportional to the Bose-Einstein function evaluated at the temperature of the sample,

$$\Theta(\omega, T_S) = \frac{\hbar\omega}{2} + \frac{\hbar\omega}{\exp[\hbar\omega/(k_B T_S)] - 1}. \quad (2)$$

Now assume that a nanoparticle with electric polarizability tensor $\alpha^E(\omega)$ is brought into this fluctuating near field at a position \mathbf{r} , such that its distance from the surface still remains appreciably larger than its characteristic linear size, while that size should be smaller than the thermal wavelength at T_S . Then the field introduces a dipole moment $\mathbf{p}(t)$ in the particle which in its turn interacts with the field, such that the power

$$\begin{aligned} & \langle \dot{\mathbf{p}}(t) \cdot \mathbf{E}(t) \rangle \\ &= \int_{-\infty}^{+\infty} d\omega (-i\omega) \frac{\varepsilon_0}{(2\pi)^2} \text{tr} \left(\alpha^E(\omega) \cdot W^E(\mathbf{r}, \mathbf{r}, \omega) \right) \end{aligned} \quad (3)$$

is dissipated in the particle, resulting in its heating. The right-hand side of this equation still is written in a manner which shows that it does not depend on the choice of the particular coordinate system used for its evaluation, as the trace over the product of the polarization tensor and the correlation tensor manifestly remains invariant under coordinate transformations. When adopting a coordinate system in which the tensor $\alpha^E(\omega)$ is diagonal, with diagonal elements $\alpha_k^E(\omega)$, this expression (3) takes the more familiar form [21–24]

$$\begin{aligned} & \langle \dot{\mathbf{p}}(t) \cdot \mathbf{E}(t) \rangle \\ &= 2 \sum_{k=1}^3 \int_0^{+\infty} d\omega \omega \text{Im}(\alpha_k^E(\omega)) \frac{\varepsilon_0}{(2\pi)^2} W_{kk}^E(\mathbf{r}, \mathbf{r}, \omega). \end{aligned} \quad (4)$$

It is essential to keep in mind that here the diagonal components $W_{kk}^E(\mathbf{r}, \mathbf{r}, \omega)$ of the sample's field correlation are given in the principal-axis system of the particle's polarizability, not in a system attached to the sample's geometry or orientation. If all elements $\alpha_k^E(\omega)$ are equal, as in the case of a nanosphere, the integrand simply is proportional to the trace of the correlation tensor, *i.e.*, to the spectral energy density

$$\langle u^E(\mathbf{r}, \omega) \rangle = \frac{\varepsilon_0}{(2\pi)^2} \sum_{k=1}^3 W_{kk}^E(\mathbf{r}, \mathbf{r}, \omega), \quad (5)$$

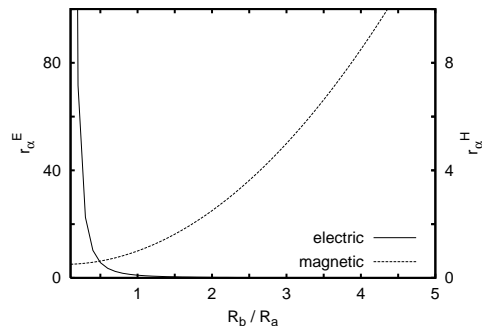


FIG. 1: Ratios $r_\alpha^{E/H} \equiv \text{Im}(\alpha_a^{E/H})/\text{Im}(\alpha_b^{E/H})$ for a spheroidal gold nanoparticle at $\omega_{\text{th}} = 10^{14} \text{ s}^{-1}$. The particle's volume is kept constant when the aspect ratio R_b/R_a is varied.

which is the case considered usually [21–24]. If, however, the elements $\alpha_k^E(\omega)$ differ significantly from each other, the dissipated power can be dominated by individual components $W_{kk}^E(\mathbf{r}, \mathbf{r}, \omega)$. This is the principle we are going to explore.

For obtaining a convenient expression for the net power flow $P_{S \leftrightarrow P}$ between the nanoparticle and the substrate, we factorize the correlation tensor in the form

$$\frac{\varepsilon_0}{(2\pi)^2} W_{kk}^E(\mathbf{r}, \mathbf{r}, \omega) = \Theta(\omega, T_S) D_{kk}^E(\mathbf{r}, \omega), \quad (6)$$

so that the quantities $D_{kk}^E(\mathbf{r}, \omega)$ carry the same dimension (sm^{-3}) as the local density of states (LDOS) [25]. Then two additional mechanisms have to be accounted for: On the one hand, as strongly emphasized by Dedkov and Kyasov [23] and by Chapuis *et al.* [24], the magnetic part $\mathbf{H}(\mathbf{r}, t)$ of the fluctuating near field gives rise to the induction of an effective magnetic dipole $\mathbf{m}_{\text{eff}}(t)$ in the particle, and hence to a further contribution $\langle \dot{\mathbf{m}}_{\text{eff}}(t) \cdot \mathbf{H}(t) \rangle$ to the dissipated energy. On the other hand, there also is a flow of energy from the particle, with temperature T_P , to the sample. In total, this results in the formula

$$\begin{aligned} P_{S \leftrightarrow P} &= 2 \sum_{k=1}^3 \int_0^{+\infty} d\omega \omega \left(\Theta(\omega, T_S) - \Theta(\omega, T_P) \right) \\ &\times \left(\text{Im}(\alpha_k^E(\omega)) D_{kk}^E(\mathbf{r}, \omega) + \text{Im}(\alpha_k^H(\omega)) D_{kk}^H(\mathbf{r}, \omega) \right). \end{aligned} \quad (7)$$

Here we assume that the principal-axis system of the magnetic polarizability tensor $\alpha^H(\omega)$ coincides with that of its electric counterpart. A particularly favorable case occurs for spheroidal nanoparticles (*i.e.*, for rotational ellipsoids with two equal semi-axes R_b and a different third semi-axis R_a), for which the polarizabilities $\alpha_k^E(\omega)$ and $\alpha_k^H(\omega)$ are known analytically [26]. In Fig. 1 we plot the ratios $r_\alpha^{E/H} \equiv \text{Im}(\alpha_a^{E/H})/\text{Im}(\alpha_b^{E/H})$ of the absorptivities along (a) and perpendicular to (b) the axis of rotation for spheroidal Au nanoparticles at the frequency $\omega_{\text{th}} = 10^{14} \text{ s}^{-1}$, roughly corresponding to the dominant thermal frequency at $T = 300 \text{ K}$. We employ the Drude

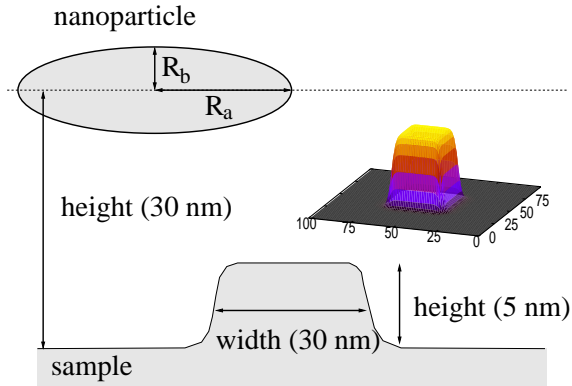


FIG. 2: Cross section, and 3D plot, of the surface structure employed in the numerical model calculations. The orientation of the spheroidal nanoparticle here corresponds to the scan of the near-field heat transfer shown in the later Fig. 5.

model

$$\varepsilon(\omega) = 1 - \frac{\omega_p^2}{\omega^2 + i\gamma\omega} \quad (8)$$

for the permittivity, with plasma frequency $\omega_p = 1.4 \cdot 10^{16} \text{ s}^{-1}$ and relaxation rate $\gamma = 3.3 \cdot 10^{13} \text{ s}^{-1}$ for gold at room temperature, and keep the particle's volume constant when varying the aspect ratio R_b/R_a . As expected, one observes $r_\alpha^E \gg 1$ for prolate, rice grain-like particles ($R_b/R_a \ll 1$), whereas $r_\alpha^H \gg 1$ for strongly oblate, pancake-like particles ($R_b/R_a \gg 1$), in which the magnetic fields can easily induce eddy currents. We expect that the model yields reliable results at least in the interval $1/5 \leq R_b/R_a \leq 5$ of the aspect ratio [27].

III. NUMERICAL MODEL CALCULATIONS

For our model calculations we take a substrate which is perfectly flat except for a square pad with 5 nm height, 30 nm width, and rounded edges, as depicted in Fig. 2. The coordinate system is oriented such that the x - y -plane coincides with the base substrate plane; the x - and y -axes being parallel to the pad's edges. We again assume that the permittivity of the substrate is described by the Drude model with parameters appropriate for gold.

In Fig. 3 a) – c) we show the “electric” elements $D_{kk}^E(\mathbf{r}, \omega)$ as defined by Eq. (6), evaluated for $\omega = \omega_{\text{th}}$ at a distance of 30 nm above the base substrate plane. These elements have been computed by means of a perturbative approach to first order in the surface profile [28]. The sum of these three quantities gives the electric part of the LDOS, plotted in Fig. 3 d). Whereas the LDOS merely yields a blurred image of the underlying surface topography [20], the individual diagonal elements $D_{kk}^E(\mathbf{r}, \omega)$ contain interesting directional information. The corresponding results for the “magnetic” elements $D_{kk}^H(\mathbf{r}, \omega)$ are shown in Fig. 4.

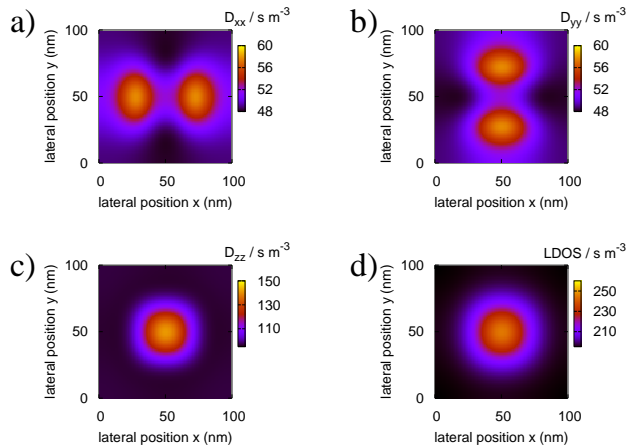


FIG. 3: a) – c): “Electric” elements $D_{kk}^E(\mathbf{r}, \omega)$ ($k = x, y, z$) for the model surface depicted in Fig. 2, computed for $\omega_{\text{th}} = 10^{14} \text{ s}^{-1}$ at a distance of 30 nm above the base x - y -plane. The dielectric properties of the substrate are given by the Drude permittivity with parameters for gold. d): Electric LDOS, as corresponding to the sum of a) – c).

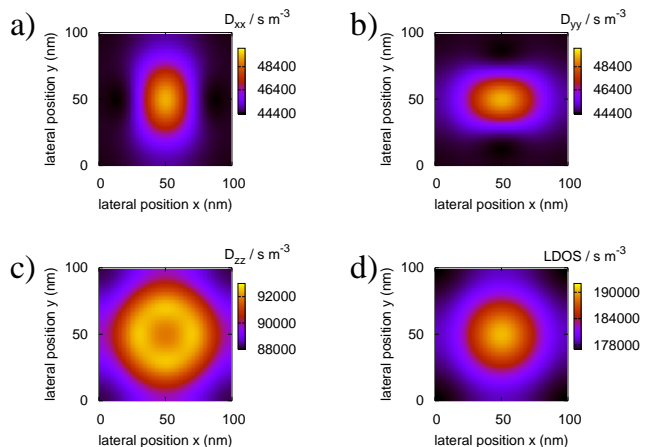


FIG. 4: As Fig. 3, for the “magnetic” elements $D_{kk}^H(\mathbf{r}, \omega)$. Observe that the scales differ from those in Fig. 3.

For understanding the message contained in these figures, it is helpful to also consider the normalized eigenvectors $\mathbf{f}^{(j)}(\mathbf{r}, \omega)$ of the 3×3 -matrix $D^E(\mathbf{r}, \omega)$, and the corresponding eigenvalues $d^{(j)}(\mathbf{r}, \omega)$, together with their magnetic counterparts [29]. Intuitively speaking, the eigenvectors give the principal directions of the local field fluctuations; of course, these directions are determined by the surface profile. The eigenvalues then specify the strength of the partial fluctuation associated with the respective principal direction. In compact matrix notation, one now has

$$D^E(\mathbf{r}, \omega) = S d S^\dagger, \quad (9)$$

where the j th column of the matrix S is given by the vector $\mathbf{f}^{(j)}(\mathbf{r}, \omega)$, the matrix S^\dagger is the adjoint of S , and d

is the diagonal matrix with $d^{(j)}(\mathbf{r}, \omega)$ at the j th position on the diagonal line. Written out in components, this implies

$$D_{kk}^E(\mathbf{r}, \omega) = \sum_{j=1}^3 d^{(j)}(\mathbf{r}, \omega) |f_k^{(j)}(\mathbf{r}, \omega)|^2. \quad (10)$$

The square $|f_k^{(j)}(\mathbf{r}, \omega)|^2$ obviously specifies the weight with which the eigenvalue $d^{(j)}(\mathbf{r}, \omega)$ contributes to the fluctuations along the k -direction. Thus, the individual diagonal elements $D_{kk}^E(\mathbf{r}, \omega)$ express the distribution of the entire fluctuation strength, which in this language corresponds to the sum $\sum_{j=1}^3 d^{(j)}(\mathbf{r}, \omega)$ and thus is proportional to the electric energy density (5), over the individual directions. Analogous remarks apply to the magnetic fluctuations. This kind of directional information is, in principle, contained in the thermal near field above a nanostructured surface, and allows one to deduce properties of the structure itself. The experimental task is to actually extract such information from given laboratory samples, and the theoretical task is to devise methods for doing so.

To this aim, we suggest a further development of the NSThM: The tip of this instrument is functionalized to act as a thermocouple, so that the small temperature change resulting from the energy deposited in or drawn out of the tip translates into a measurable voltage [11–13]. If the active volume could be given the shape of a spheroid, the shape-dependence of the heat transfer expressed by Fig. 1 could be exploited for assessing individual elements $D_{kk}^{E/H}(\mathbf{r}, \omega)$ by means of Eq. (7). Additional experimental handles would then be provided by the choice of both the spheroid's orientation and its material.

In order to demonstrate the feasibility of this concept, we compute the near-field heat transfer between our model gold substrate with temperature $T_S = 300$ K and spheroidal nanoparticles cooled down to $T_P = 100$ K. For metallic nanoparticles the magnetic contribution to the total heat transfer generally is much larger than the electric one [23, 24], so that one has to select non-metallic sensors when aiming at the electric components $D_{kk}^E(\mathbf{r}, \omega)$. Here we consider a rice grain-like particle with the permittivity of gallium nitride (GaN), described by the formula [30]

$$\epsilon(\omega) = \epsilon_\infty + \frac{S\omega_0^2}{\omega_0^2 - \omega^2 - i\Gamma\omega} - \frac{\omega_n^2}{\omega^2 + i\gamma\omega} \quad (11)$$

with parameters $\epsilon_\infty = 5.4$, $S = 5.1$, $\omega_0 = 1.0 \times 10^{14} \text{ s}^{-1}$, $\omega_n = 9.1 \times 10^{14} \text{ s}^{-1}$, $\Gamma = 2.7 \times 10^{12} \text{ s}^{-1}$, and $\gamma = 7.1 \times 10^{14} \text{ s}^{-1}$; the values of the inverse relaxation times Γ and γ have been properly adjusted to the particle's temperature. We choose the half-axes $R_a = 40$ nm and $R_b = 10$ nm, so that $r_\alpha^E \approx 23.4$ at ω_{th} . These parameters clearly fall outside the regime where the dipole model (7) can give quantitatively accurate results. We employ this

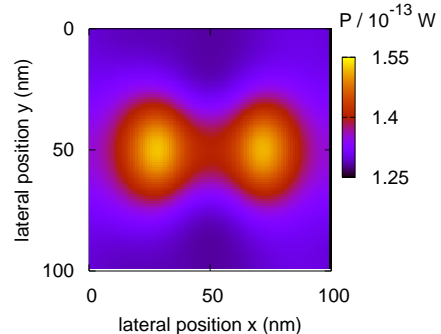


FIG. 5: Total heat transfer between a cooled spheroidal GaN nanoparticle ($T_P = 100$ K) with $R_a = 40$ nm, $R_b = 10$ nm, and axis of rotation parallel to the x -axis, and the gold structure sketched in Fig. 2 ($T_S = 300$ K), assuming that the particle is scanning the structure with a constant height of 30 nm.

model nonetheless, as computational tools for calculating the near-field heat transfer between nanoparticles and structured surfaces are not yet available, and stress the qualitative nature of the following results.

Figure 5 shows the total heat transfer according to the model (7), with the particle oriented parallel to the x -axis at a constant height of 30 nm above the base plane while scanning the substrate, as previously sketched in Fig. 2. In this case the heat flux mainly picks up the contribution proportional to $D_{xx}^E(\mathbf{r}, \omega_{\text{th}})$. As a consequence, the signal obtained here closely resembles the previous Fig. 3 a). The slight differences between the two figures visible above the pad's center are explained by the fact that $D_{zz}^E(\mathbf{r}, \omega_{\text{th}})$ contributes significantly here.

For assessing the magnetic contributions, we select a pancake-like Au nanospheroid with $R_a = 10$ nm and $R_b = 40$ nm, giving $r_\alpha^H \approx 8.5$, and orient it along the z -axis. The total heat transfer then is dominated by $D_{zz}^H(\mathbf{r}, \omega_{\text{th}})$, as witnessed by the good agreement of Fig. 6 with 4 c). Thus, here the recorded heat flux provides information on a component of the magnetic correlation tensor.

IV. CONCLUSION

In this paper we have outlined that individual diagonal components of the correlation tensors of fluctuating thermal fields close to the surface of a given material can be measured by near-field thermal imaging, if the sensor employed for recording the heat flux is appropriately shaped. Evidently this proposal still is somewhat sketchy and idealized: On the theoretical side, there is an urgent need for accurate computational tools for quantifying the near-field heat flux between arbitrarily shaped nanoparticles and structured surfaces; from the experimental viewpoint, the development of the required sensors poses a serious challenge. Thus, there may still be a

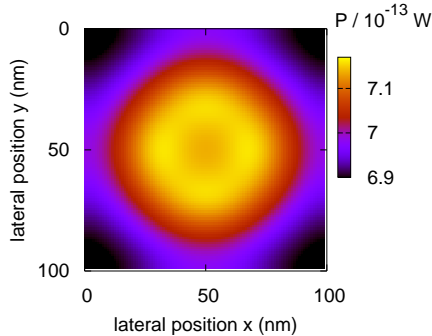


FIG. 6: Total heat transfer between a cooled spheroidal Au nanoparticle ($T_P = 100$ K) with $R_a = 10$ nm, $R_b = 40$ nm, and axis of rotation parallel to the z -axis, and the gold structure sketched in Fig. 2 ($T_S = 300$ K), assuming that the particle is scanning the structure with a constant height of 30 nm.

long way from our present matter-of-principle considerations to laboratory applications.

Yet, there are at least two reasons for exploring this option. First, fluctuational electrodynamics is a macroscopic theory; it would be important to test its predic-

tions even for probe-sample distances of a few nanometers and below, where its validity can no longer be taken for granted. Possible deviations from the macroscopic theory would then yield important novel insight into fundamental processes in dielectrics. For this program sensitive observables are required; we suggest that measuring individual diagonal components of the near fields' correlation tensors, which give directional weights to the total fluctuation strength, might yield more information than their traces, *i.e.*, the local density of states. Second, leaving theoretical considerations aside, the practical exploitation of the principles outlined in this note for nanoscale thermal imaging [20] would provide novel tools for the diagnosis and characterization of nanostructures.

Acknowledgments

This work was supported by the Deutsche Forschungsgemeinschaft through Grant No. KI 438/8-1. Computer power was obtained from the GOLEM I cluster of the Universität Oldenburg. S.-A. B. gratefully acknowledges support from the Deutsche Akademie der Naturforscher Leopoldina under Grant No. LPDS 2009-7.

-
- [1] S. M. Rytov, Yu. A. Kravtsov, and V. I. Tatarskii, *Principles of Statistical Radiophysics* (Springer, Berlin, 1989).
 - [2] D. Polder and M. van Hove, *Phys. Rev. B* **4**, 3303 (1971).
 - [3] K. Joulain, J.-P. Mulet, F. Marquier, R. Carminati, and J.-J. Greffet, *Surf. Sci. Rep.* **57**, 59 (2005).
 - [4] A. I. Volokitin and B. N. J. Persson, *Rev. Mod. Phys.* **79**, 1291 (2007).
 - [5] L. Hu, A. Narayanaswamy, X. Chen, and G. Chen, *Appl. Phys. Lett.* **92**, 133106 (2008).
 - [6] A. Narayanaswamy, S. Shen, and G. Chen, *Phys. Rev. B* **78**, 115303 (2008).
 - [7] S. Shen, A. Narayanaswamy, and G. Chen, *Nano Lett.* **9**, 2909 (2009).
 - [8] E. Rousseau, A. Siria, G. Jourdan, S. Volz, F. Comin, J. Chevrier, and J.-J. Greffet, *Nature Photonics* **3**, 514 (2009).
 - [9] C. Henkel and K. Joulain, *Appl. Phys. B* **84**, 61 (2006).
 - [10] P.-O. Chapuis, S. Volz, C. Henkel, K. Joulain, and J.-J. Greffet, *Phys. Rev. B* **77**, 035431 (2008).
 - [11] W. Müller-Hirsch, A. Kraft, M. T. Hirsch, J. Parisi, and A. Kittel, *J. Vac. Sci. Technol. A* **17**, 1205 (1999).
 - [12] A. Kittel, W. Müller-Hirsch, J. Parisi, S.-A. Biehs, D. Reddig, and M. Holthaus, *Phys. Rev. Lett.* **95**, 224301 (2005).
 - [13] U. F. Wischnath, J. Welker, M. Munzel, and A. Kittel, *Rev. Sci. Instrum.* **79**, 073708 (2008).
 - [14] Y. De Wilde, F. Formanek, R. Carminati, B. Gralak, P.-A. Lemoine, K. Joulain, J.-P. Mulet, Y. Chen, and J.-J. Greffet, *Nature* **444**, 740 (2006).
 - [15] R. S. DiMatteo, P. Greiff, S. L. Finberg, K. A. Young-Waithe, H. K. H. Choy, M. M. Masaki, and C. G. Fonstad, *Appl. Phys. Lett.* **79**, 1894 (2001).
 - [16] A. Narayanaswamy and G. Chen, *Appl. Phys. Lett.* **82**, 3544 (2003).
 - [17] M. Laroche, R. Carminati, and J.-J. Greffet, *J. Appl. Phys.* **100**, 063704 (2006).
 - [18] M. Francoeur, M. P. Mengüç, and R. Vaillon, *Appl. Phys. Lett.* **93**, 043109 (2008).
 - [19] S. Basu, Z. M. Zhang, and C. J. Fu, *Int. J. Energy Res.* **33**, 1203 (2009).
 - [20] A. Kittel, U. F. Wischnath, J. Welker, O. Huth, F. Rüting, and S.-A. Biehs, *Appl. Phys. Lett.* **93**, 193109 (2008).
 - [21] I. A. Dorofeyev, *J. Phys. D: Appl. Phys.* **31**, 600 (1998).
 - [22] J. B. Pendry, *J. Phys.: Condens. Matter* **11**, 6621 (1999).
 - [23] G. V. Dedkov and A. A. Kyasov, *Tech. Phys. Lett.* **33**, 305 (2007).
 - [24] P.-O. Chapuis, M. Laroche, S. Volz, and J.-J. Greffet, *Phys. Rev. B* **77**, 125402 (2008).
 - [25] K. Joulain, R. Carminati, J.-P. Mulet, and J.-J. Greffet, *Phys. Rev. B* **68**, 245405 (2003).
 - [26] L. D. Landau, E. M. Lifshitz, and L. P. Pitaevskii, *Electrodynamics of Continuous Media*, Landau and Lifshitz Course of Theoretical Physics, Volume 8 (Butterworth-Heinemann, Oxford, 2000).
 - [27] O. Huth, F. Rüting, S.-A. Biehs, and M. Holthaus, *Eur. Phys. J. Appl. Phys.* **50**, 10603 (2010).
 - [28] S.-A. Biehs, O. Huth, and F. Rüting, *Phys. Rev. B* **78**, 085414 (2008).
 - [29] B. Zhang and C. Henkel, *J. Appl. Phys.* **102**, 084907 (2007).
 - [30] A. S. Barker and M. Ilegems, *Phys. Rev. B* **7**, 743 (1973).